Journal of Orthopaedic Translation 44 (2024) 88–101

Contents lists available at ScienceDirect

Journal of Orthopaedic Translation

journal homepage: www.journals.elsevier.com/journal-of-orthopaedic-translation

Original Article

Targeting FGFR3 signaling and drug repurposing for the treatment of SLC26A2-related chondrodysplasia in mouse model

Pan Li [a,b,1], Dong Wang [a,c,1], Weiguang Lu [a,1], Xin He [c], Jingyan Hu [d], Haitao Yun [a], Chengxiang Zhao [a], Liu Yang [a,b], Qiang Jie [e,**], Zhuojing Luo [a,b,*]

[a] Institute of Orthopedic Surgery, Xijing Hospital, Fourth Military Medical University, Xi'an, China
[b] Medical Research Institute, Northwestern Polytechnical University, Xi'an, China
[c] Department of Medicine Chemistry and Pharmaceutical Analysis, School of Pharmacy, Fourth Military Medical University, Xi'an, China
[d] Department of Biology, Northwestern University, Xi'an, China
[e] Department of Orthopedic Surgery, HongHui Hospital, Xi'an Jiaotong University, College of Medicine, Xi'an, China

ARTICLE INFO

Keywords:
SLC26A2
Chondrodysplasia
FGFR3 signaling
NVP-BGJ398
Drug repurposing

ABSTRACT

Background: Mutations in Slc26a2 cause a spectrum of autosomal-recessive chondrodysplasia with a significant and negligible influence on the quality of life. It has been reported that Slc26a2 deficiency triggers the ATF6 branch of the UPR, which may, in turn, activate the negative regulator of the FGFR3 signaling pathway. However, the correlation between the deletion of Slc26a2 and the augmentation of downstream phosphorylation of FGFR3 has not been investigated *in vivo*.

Methods: First, we constructed *Slc26a2* and *Fgfr3* double knockout mouse lines and observed gross views of the born mice and histological staining of the tibial growth plates. The second approach was to construct tamoxifen-inducible *Cre-ER^{T2}* mouse models to replicate SLC26A2-related non-lethal dysplastic conditions. Pharmacological intervention was performed by administering the FGFR3 inhibitor NVP-BGJ398. The effect of NVP-BGJ398 on chondrocytes was assessed by Alcian blue staining, proliferation, apoptosis, and chondrocyte-specific markers and then verified by western blotting for variations in the downstream markers of FGFR3. The growth process was detected using X-rays, micro-CT examination, histomorphometry staining of growth plates, and immunofluorescence.

Results: Genetic ablation of *Fgfr3* in embryonic *Slc26a2*-deficient chondrocytes slightly attenuated chondrodysplasia. Subsequently, in the constructed mild dysplasia model, we found that postnatal intervention with *Fgfr3* gene in *Slc26a2*-deficient chondrocytes partially alleviated chondrodysplasia. In chondrocyte assays, NVP-BGJ398 suppressed the defective phenotype of *Slc26a2*-deficient chondrocytes and restored the phosphorylation downstream of FGFR3 in a concentration-dependent manner. In addition, *in vivo* experiments showed significant alleviation of impaired chondrocyte differentiation, and micro-CT analysis showed a clear improvement in trabecular bone microarchitectural parameters.

Conclusion: Our results suggested that inhibition of FGFR3 signaling pathway overactivation and NVP-BGJ398 has promising therapeutic implications for the development of SLC26A2-related skeletal diseases in humans.

The translational potential of this article: Our data provide genetic and pharmacological evidence that targeting FGFR3 signaling via NVP-BGJ398 could be a route for the treatment of SLC26A2-associated skeletal disorders, which promisingly advances translational applications and therapeutic development.

Abbreviations: ACG1B, achondrogenesis type IB; AO2, atelosteogenesis type 2; BMD, bone mineral density; BV/TV, bone volume relative to total tissue volume; DTD, diastrophic dysplasia; ER stress, endoplasmic reticulum stress; Micro-CT, micro-computed tomography; rMED, recessive multiple epiphyseal dysplasia; Tb.N, trabecular number; Tb.Sp, trabecular bone separation; Tb.Th, trabecular thickness; UPR, unfolded protein response.

* Corresponding author. Institute of Orthopedic Surgery, Xijing Hospital, Fourth Military Medical University, Xi'an, China.
** Corresponding author.
E-mail addresses: lipan666222@hotmail.com (P. Li), wangdongfmmu@hotmail.com (D. Wang), luweiguang1989@126.com (W. Lu), 1543618464@qq.com (X. He), hujingyan0910@163.com (J. Hu), yunhaitao_1@163.com (H. Yun), 357961940@qq.com (C. Zhao), yangliu@fmmu.edu.cn (L. Yang), jieqiangchina@126.com (Q. Jie), zjluo@fmmu.edu.cn (Z. Luo).

[1] Pan Li, Dong Wang and Weiguang Lu contributed equally.

https://doi.org/10.1016/j.jot.2023.09.003
Received 24 December 2022; Received in revised form 18 August 2023; Accepted 20 September 2023

2214-031X/© 2023 Published by Elsevier B.V. on behalf of Chinese Speaking Orthopaedic Society. This is an open access article under the CC BY-NC-ND license (http://creativecommons.org/licenses/by-nc-nd/4.0/).

1. Introduction

The Slc26a2-encoded cell transmembrane sulfate transporter plays a vital role in chondrocyte proliferation, differentiation, and maturation [1]. Mutations in Slc26a2 cause a spectrum of autosomal-recessive chondrodysplasia conditions, including the lethal forms of achondrogenesis type IB (ACG1B) and atelosteogenesis type 2 (AO2), the milder end of the spectrum of diastrophic dysplasia (DTD), recessive multiple epiphyseal dysplasia (rMED), and dysplastic spondylolysis [2–4]. Dysplasia caused by Slc26a2-related skeletal disorders remains incurable [5,6]. Therefore, there is an urgent need to explore the mechanisms and identify new therapeutic targets for pharmacological treatments.

SLC26A2-associated cartilage diseases are classified as perinatally lethal chondrodysplasia and milder postnatal skeletal disorders [7]. The severity of the clinical phenotype was reported to correlate with the residual capacity of sulfate transporters [8]. Regarding SLC26A2-related deficiency causing dysplasia, the first model animal of a mouse strain with a mutation in the *Slc26a2 gene* (*dtd* mouse) was constructed by Antonio Rossi et al. which provided a valuable model to explore the pathogenesis and therapeutic aspects of human catastrophic dysplasia [9]. A series of studies in their *dtd mice* found that insufficient proteoglycan sulfation led to a "diffuse loss" of growth signaling molecules in the cartilage matrix and that the lack of sulfation of the C4S site in chondroitin sulfate resulted in reduced binding to the secretory protein Indian hedgehog (Ihh) [10].

Previously, by globally and conditionally deleting *Slc26a2* in mice, we phenocopied the two most severe lethal human diseases and found that deficient collagen secretion in chondrocytes triggers the ATF6 arm of the UPR [6]. The transcription factor ATF6 further transcriptionally regulated FGFR3 through regulatory elements, and activated FGFR3 initiates intracellular signaling cascades that control various physiological functions, including cell differentiation, proliferation, survival, migration, embryonic development, and angiogenesis [11]. Indeed, our pre-trial found that administration of the FGFR3 inhibitor NVP-BGJ398 to pregnant females elicited therapeutic effects on the pathological features of $Slc26a2^{-/-}$ neonates [6]. However, no studies have verified the correlation between the deletion of SLC26A2 and the augmentation of downstream phosphorylation of FGFR3 *in vivo*.

In light of the fact that the spectrum of diseases caused by Slc26a2 gene defects is broad, we are particularly concerned with postnatal chondrodysplasia typology in clinical practice. In these phenotypes we have observed a similar association between *Slc26a2* deletion and FGFR3 downstream phosphorylation. Additionally, the knockdown of *Fgfr3* alleviated the malformation pattern of *Slc26a2* deletion. Previous studies have suggested that FGFR3 primarily inhibits chondrocyte proliferation through the STAT1-p21 pathway and chondrocyte differentiation through the ERK-MAPK pathway. A study conducted by Mahdia Taieb revealed that deletion mutations in the xylosyltransferase I gene, responsible for facilitating the synthesis of proteoglycans, lead to an increase in FGFR3 expression and activation of the ERK1/2 signaling pathway [12]. Given that FGFR3 activation is associated with chondrodysplasia, the most common form of chondrogenesis in humans, the $Fgfr3^{G369C/+}$ mice mimicking human achondroplasia exhibited a significant reduction in hypertrophic chondrocytes and narrowing of the hypertrophic band. These changes were accompanied by a marked decrease in collagen X expression. NVP-BGJ398 is a potent and selective pan-FGFR kinase inhibitor that has demonstrated antitumor activity in patients with FGFR2-altered advanced cholangiocarcinoma and promotes tumor reduction in patients with FGFR1-amplified breast cancer [13]. In animal experiments, it was shown that NVP-BGJ398 could reduce FGFR3 phosphorylation and correct pathological hallmarks in the $Fgfr3^{Y367C/+}$ mouse model [14]. Most importantly, NVP-BGJ398 is currently being tested in the clinical setting to treat FGFR3-related pediatric achondroplasia [15]. Therefore, we speculated that NVP-BGJ398 is a promising translatable drug for the treatment of *Slc26a2* deficiency-related dysplasia.

Here, we showed for the first time that genetic ablation of *Fgfr3* in *Slc26a2*-deficient chondrocytes partially alleviates chondrodysplasia. Furthermore, tamoxifen-induced *Slc26a2* knockout mice were constructed to replicate non-lethal dysplastic conditions. We confirmed that inhibition of the FGFR3 signaling pathway and subcutaneous injection of the FGFR3 inhibitor NVP-BGJ398 promoted cartilage growth in dysplastic mice. After the pharmacological intervention, the skeletal disorders of *mutant mice* were ameliorated, and the tibial bending deformity was restored. There was a pronounced alleviation of impaired cartilage differentiation, and the micro-CT analysis results indicated that the trabecular bone microarchitecture parameters were significantly improved. Our results suggested that the inhibition of FGFR3 signaling pathway overactivation and NVP-BGJ398 have promising therapeutic implications for developing SLC26A2-related DTD and rMED diseases in humans.

2. Materials and methods

2.1. Animal models

To generate *Col2a1-Cre; Slc26a2*$^{fl/fl}$*; Fgfr3*$^{fl/fl}$ mice, the *Slc26a2*-LoxP mouse line was genotyped by PCR using primers flanking the LoxP site (5′-GCAACACTATCTCTCTGCTTGGCCT-3′ and 5′-ACCACTAAGGATTCTCCCGTGCAT-3′). The *Fgfr3*-LoxP mouse line was kindly donated by Prof. Lin Chen, Center of Bone Metabolism and Repair, Daping Hospital, Third Military Medical University [16]. *Col2a1-Cre* mice were kindly donated by Prof. Xiaochun Bai, Department of Orthopaedics, Southern Medical University [17], and *Col2a1-CreER*^{T2} was kindly provided by Prof. Di Chen, Department of Biochemistry, Rush University Medical Center [18]. The potential effects of mouse genetic background were minimized by crossing the mouse lines used in this study with wild-type C57BL/6 mice for N9 generations prior to any evaluation. Animal care and experiments were conducted in conformance with protocols approved by the Animal Research Ethics Committee of the Fourth Military Medical University.

2.2. Skeletal preparation and safranin O staining

For whole-mount skeletal staining, the neonates were collected immediately after birth and fixed overnight in 95% ethanol at room temperature. The specimens were then placed in acetone at room temperature overnight and immersed in a cartilage staining solution containing 0.03% (w/v) Alcian blue, 80% ethanol, and 20% acetic acid. The initial washing was performed using several changes in 70% ethanol to disrupt the cartilage. To better observe cartilage morphology, washing was terminated before the cartilage was completely stained. The ossified tissues were stained with alizarin red solution containing 0.005% (w/v) alizarin red in 1% (w/v) KOH for 4 h at room temperature and then sequentially incubated overnight at 4 °C to retard the staining rate. The samples were placed in 50% glycerol solution containing 1% (w/v) KOH to eliminate excessive staining [19]. Finally, the images of the stained skeleton were acquired under a dissecting microscope using bright-field optics. For Safranin O staining, tibial tissues were fixed overnight in 4% paraformaldehyde, followed by gradual decalcification and dehydration. Tissue was encapsulated in OCT compound (Leica) and sequentially cut into 8-μm frozen sections, stained with Safranin O [20].

2.3. Primary chondrocyte culture

For the primary culture of chondrocytes, rib cartilage was isolated from E18.5 embryos and digested with 3 mg per ml collagenase D (Roche) solution for 40 min at 37 °C under 5% CO2 in a thermal incubator. The tissue fragments were agitated several times to separate the soft tissues and transferred to 0.5 mg per ml of collagenase D solution at 37 °C overnight. The digestion solution was retrieved, filtered through a 40 μm cell strainer, and centrifuged for 10 min at 500×*g*. The pellet was

resuspended with DMEM (Sigma Aldrich) supplemented with 10% fetal bovine serum (Gbico), 2 μM L-GIn, 50 U per ml penicillin, and 0.05 mg per ml streptomycin. Rib chondrocytes were seeded at a density of 25 × 10^3 cells per cm^2 and cultured under sterile conditions at 37 °C and 5% CO2.

2.4. The CCK-8 test for detecting cell proliferation activity

Cell proliferation was measured using a Cell Counting Kit-8 (CCK8) assay (Cell Counting Kit 8, Beyotime, Shanghai, China) according to the manufacturer's instructions. Primary chondrocytes were inoculated into 96-well plates at a density of 5000 cells per well and incubated at 37 °C and 5% CO_2 until the cells were attached to the wall. After 72 h of incubation at 37 °C and 5% CO_2, 10 μl CCK-8 solution was added to each well and incubated at 37 °C and 5% CO_2 for 1 h. The absorbance of each sample was measured at 450 nm by measuring the OD value of living cells using a microplate reader.

2.5. Cell viability

To explore the effect of NVP-BGJ398 on the viability of primary chondrocytes, the cells were treated with different concentrations of NVP-BGJ398 (0.1, 1, 5, and 10 μM) and then incubated at 37 °C and 5% CO_2 for 72 h. The cell viability assay was performed 4 h after the addition of the MTT solution.

2.6. TUNEL assay

Apoptotic cells were detected in situ on cryosections of the tibia by the TUNEL method using the In Situ Cell Death Detection Kit (Roche) according to the manufacturer's instructions [21].

2.7. Immunostaining

Immunofluorescence analysis of the frozen sections of the tibia was performed as previously described. The following primary antibodies used were Ki67 (Millipore, Burlington, MA, USA), anti-Col X (Abclonal, A11645, 1:100), anti-phosphatase-ERK1/2 (Cell Signaling Technology, 4370, 1:100), anti-phosphatase-STAT1 (Cell Signaling Technology, 9172, 1:100), anti-SOX9 (Abcam, ab185966, 1:100), anti-Col2α1 (Thermo Fisher, PA1-26206, 1:100), and anti-aggrecan (Thermo Fisher, MA3-16,888, 1:100). Alexa Fluor 594 concanavalin A (Invitrogen) was used for colocalization with collagen. For Col X antigen retrieval, the sections were digested with 2 mg/ml hyaluronidase (Sigma Aldrich) for 20 min at 37 °C. Primary antibodies were detected using the appropriate Alexa Fluor-conjugated secondary antibody (Abcam). All sections were visualized using the ProLong Gold Antifade and examined under a fluorescence microscope (Zeiss).

2.8. Western blot and quantitative real-time RT-PCR(qPCR)

For immunoblotting assays, tissues and cells were lysed with RIPA buffer and centrifuged to obtain total protein. Protein concentrations were measured using the Pierce BCA Protein Assay Kit (Thermo Fisher Scientific). Proteins were prepared by mixing with loading buffer (Beyotime Biotechnology, China), boiled for 15 min, subjected to SDS-PAGE, and then transferred to PVDF membranes. Blots were detected with primary antibodies, including anti-glyceraldehyde 3-phosphate dehydrogenase (GAPDH) (Cell Signaling Technology, #2118, 1:1000), anti-SLC26A2 (ABclonal, A6369, 1:1000), anti-FGFR3 (Invitrogen, PA5-34,574, 1:1000), anti- ERK1/2 (Cell Signaling Technology, 9102, 1:1000), anti-phosphatase-ERK1/2 (Cell Signaling Technology, 4370, 1:1000), anti- STAT1 (Cell Signaling Technology, 9172, 1:1000), and anti-phosphatase-STAT1 (Cell Signaling Technology, 9167, 1:1000). The membranes were then incubated with horseradish peroxidase (HRP)-conjugated goat anti-rabbit IgG or horse anti-mouse IgG secondary antibody (Cell Signaling Technology, #7074 or #7076, Cell Signaling Technology) for 2 h. After each step, the membranes were washed thrice with TBS containing 0.1% Tween-20 (Tris-buffered saline) for 15 min each. Finally, the PVDF membranes were detected using Immobilon Western Chemiluminescent HRP Substrate (#WBKLS0100, Millipore, Germany) and visualized using Amersham Imager 600 (General Electric, USA). For qPCR, total RNA was extracted from tissues or cells using the MiniBEST Universal RNA Extraction Kit (TaKaRa). Reverse transcription was performed using PrimeScript RT Master Mix (TaKaRa). The synthesized cDNA was subjected to qPCR using the TB Green Premix Ex Taq II (TaKaRa Bio). The primers used for qPCR are listed in Table 1 and the results are shown in Fig. S1 and Fig. S3.

2.9. Micro-CT and three-dimensional bone mass analysis

Mouse tibias were radiographed on a Faxitron machine (MX-20). After removing excess muscle and other soft tissues, whole mouse skeleton, tibia, and femur specimens were obtained, fixed in 4% paraformaldehyde at 4 °C for one day, and then stored in 70% ethanol. The specimens were fixed in a scanning tube using a foam plate, according to the adjusted length of the specimen. The scanning protocol was set according to the following parameters: scanning resolution, 21 μm; rotation angle, 360°; rotation angle increment, 0.4°; voltage, 80 kV; current, 80 μA; exposure time, 3000 ms; frame average, 4; pixel combination, 1 × 1 (eXplore Locus SP; GE Health Care Co., USA); and black and white scanning calibration: Hounsfield scale correction and reconstruction streak normalization correction [22]. The scanned files were analyzed by 3D reconstruction using the Micview V2.1.2 3D reconstruction processing software and ABA special skeletal analysis software.

2.10. Drug treatment

4-hydroxy tamoxifen (4-OH tamoxifen), an active metabolite of tamoxifen *in vivo*, was used to treat primary chondrocytes isolated from *Col2a1-CreER^{T2}; Slc26a2$^{fl/fl}$* mice with 1 μm 4-OH tamoxifen for 48 h. NVP-BGJ398 was fused in DMSO solution to obtain different concentrations, and the final cellular drug concentration was 5 μm. To induce Cre recombination in mice, tamoxifen (Sigma–Aldrich, St. Louis, MO, USA) was solubilized in corn oil to a final concentration of 10 mg/ml. To delete *Slc26a2* in chondrocytes, *Col2a1-CreER^{T2}; Slc26a2$^{fl/fl}$* (*Slc26a2* cKO) mice and wild-type (cre-negative control, CTR) littermates were injected intraperitoneally with tamoxifen at 1 mg/10 g body weight for five consecutive days to replicate the phenotype of DTD mice from P10 [23]. The first strategy was based on the DTD dysplasia model, and we continued to construct *Col2a1-CreER^{T2}; Slc26a2 $^{fl/fl}$; Fgfr3$^{fl/fl}$* (*Slc26a2; Fgfr3* cKO) mice with continuous subcutaneous injection of tamoxifen for five days from day P10, followed by analysis at P20. The second protocol was a continuous subcutaneous injection of NVP-BGJ398 (ApexBio Technology, 2 mg/kg body weight, dissolved in 50 μl DMSO) with *Col2a1-CreER^{T2}; Slc26a2 $^{fl/fl}$* mice for 5 days from P15–P19 after induction of recombination, and mice were taken at P20 for analysis. In the

Table 1
The primers used for qPCR to confirm Cre recombination.

Gene	Primer sequences (5′-3′)
GAPDH (F)	AGCTACTCGCGGCTTTACG
GAPDH (R)	ATCCGTTCACACCGACCTTC
SLC26A2 (F)	AAGAGCAGCATGACCTCTCAC
SLC26A2 (R)	CTGCCTCAAGTCAGTGCCT
FGFR3 (F)	CCACCGACAAGGAGCTAGAGG
FGFR3 (R)	CGGTGACAGGCTTGGCAGTA
Sox9(F)	GAGTTTGACCAATACTTGCCAC
Sox9(R)	ACTGCCAGTGTAGGTGAC
Col2a1(F)	ATCTTGCCGCATCTGTGTGT
Col2a1(R)	CTCCTTTCTGCCCCTTTGGC
Aggrecan(F)	GCCTACCCGGTACCCTACAG
Aggrecan(R)	ACATTGCTCCTGGTCTGCAA

third protocol, P10 *Col2a1-CreER^{T2}; Slc26a2 $^{fl/fl}$* mice were injected intraperitoneally with tamoxifen (1 mg/10 g body weight) for five consecutive days. Tamoxifen was intraperitoneally injected every three days, and NVP-BGJ398 (2 mg/kg body weight) was administered every day, except for the day when mice were administered tamoxifen from postnatal days 20–49. The mice were analyzed on postnatal day 49 using isoflurane anesthesia.

2.11. Statistical analysis

The analysis was performed using GraphPad Prism 8.0 (GraphPad Software, USA). All data are expressed as mean ± SD. An F-test for equality of variances was performed to ensure the same variance of tested groups. The Shapiro–Wilk test or D'Agostino test was performed to determine whether the collected data follows a normal distribution. Data were analyzed by one-way ANOVA with the Tukey post hoc test to compare means among >2 groups. Here, n refers to the number of independent experiments or mice per group. Significance was defined as $P < 0.05$.

3. Results

3.1. Ablation of Fgfr3 in Col2a1-Cre; Slc26a2$^{fl/fl}$ mice ameliorates chondrodysplasia

To validate the genetic interaction between *Slc26a2* and *Fgfr3*, we constructed chondrocyte-specific *Slc26a2* and *Fgfr3* double-knockout mouse models. As previously reported, all neonatal mice with a specific knockout of *Slc26a2* in chondrocytes died after birth without any respiratory movement of the thorax. Mice with simultaneously knocked out *Slc26a2* and *Fgfr3* genes in chondrocytes showed alleviation of the shortened limb and a minor extension of postnatal survival (n > 6) (Fig. 1A). Western blot experiments verified successful Cre-mediated recombination, as evidenced by the fact that SLC26A2 protein decreased significantly in rib cartilage tissue at the P0 stage in *mutant mice*. In addition, FGFR3 protein content was significantly increased in the rib chondrocytes of *Col2a1-Cre; Slc26a2$^{fl/fl}$* mice, suggesting overactivation of the FGFR3 signaling pathway after knockout of *Slc26a2*. Excessive levels of FGFR3 were completely abolished in *Col2a1-Cre; Slc26a2$^{fl/fl}$; Fgfr3$^{fl/fl}$* mice (Fig. 1B and C). Alizarin blue/alizarin red bone staining showed that *Col2a1-Cre; Slc26a2$^{fl/fl}$; Fgfr3$^{fl/fl}$* mice had increased body length, enlarged thorax, and longer limbs than *Col2a1-Cre; Slc26a2$^{fl/fl}$* newborns. In addition, the arrangement of growth plate chondrocytes improved in *Col2a1-Cre; Slc26a2$^{fl/fl}$; Fgfr3$^{fl/fl}$* mice (Fig. 1D, E, and F). Safranin O was used to evaluate the degree of extracellular matrix sulfation [24]. Compared to the growth plates in *Col2a1-Cre; Slc26a2$^{fl/fl}$* mice, the extracellular matrix of growth plates in *Col2a1-Cre; Slc26a2$^{fl/fl}$; Fgfr3$^{fl/fl}$* mice showed a slightly deeper staining in the resting and proliferative zones, although sulfation of the matrix was not fully restored (Fig. 2A). Compared to *Col2a1-Cre; Slc26a2$^{fl/fl}$* mice, *Col2a1-Cre; Slc26a2$^{fl/fl}$; Fgfr3$^{fl/fl}$* mice showed a partially recovered growth plate structure, as evidenced by a statistically significant increase in the cell length, size, and density of chondrocytes in all three parts of the growth plates in *Col2a1-Cre; Slc26a2$^{fl/fl}$; Fgfr3$^{fl/fl}$* mice (Fig. 2B, C, D). These results demonstrated that deletion of the *Fgfr3* gene in chondrocytes ameliorates the symptoms of chondrodysplasia in *Slc26a2 mutant mice.*

3.2. Deletion of the FGFR3 ameliorates defective proliferation, apoptosis, and differentiation of growth plate chondrocytes caused by Slc26a2 deficiency

To confirm whether targeting the FGFR3 signaling pathway promotes the recovery of growth plate structures by restoring cell proliferation and apoptosis, we performed Ki67 and TUNEL immunostaining. The results

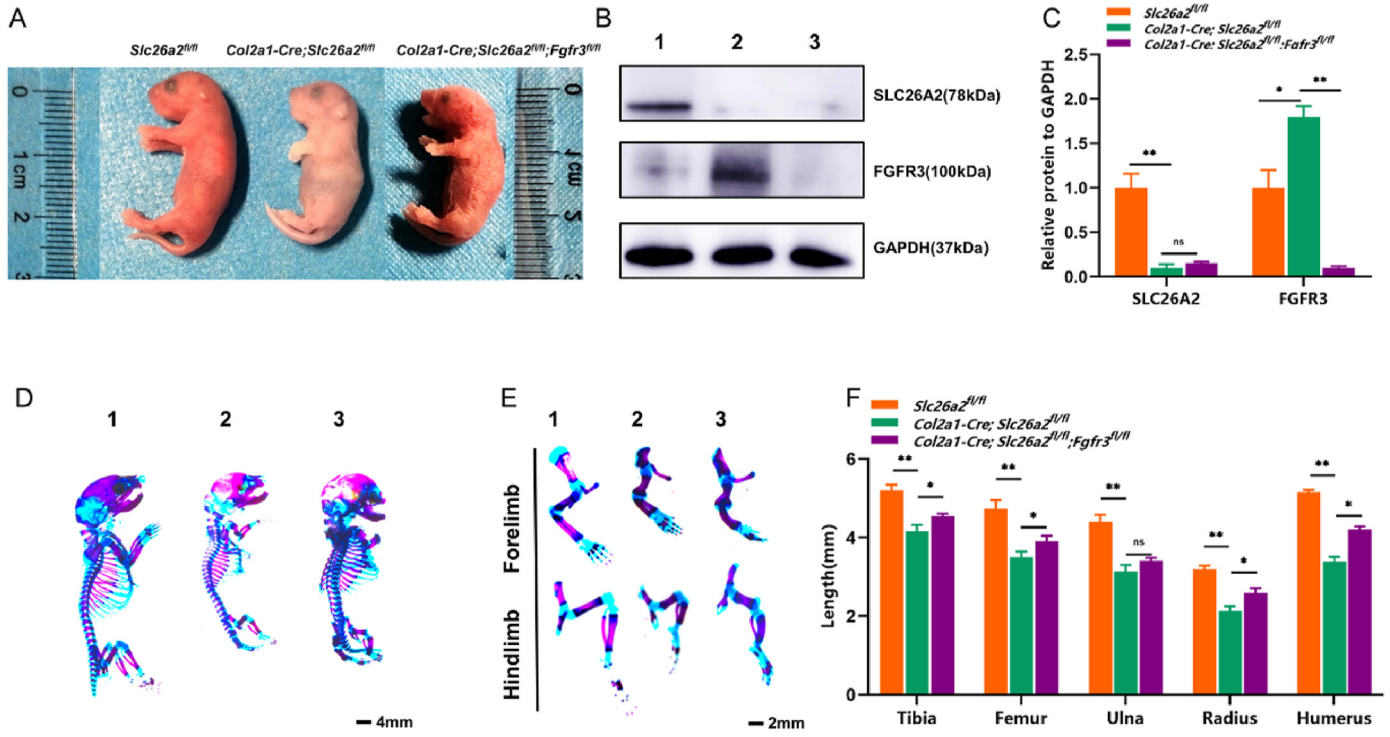

Fig. 1. Ablation of *Fgfr3* in *Col2a1-Cre; Slc26a2$^{fl/lfl}$* mice ameliorates chondrodysplasia (A) Gross appearance of *Slc26a2$^{fl/lfl}$*, *Col2a1-Cre; Slc26a2$^{fl/fl}$*, *Col2a1-Cre; Slc26a2$^{fl/fl}$; Fgfr3$^{fl/fl}$* at P0 (B) Western blotting showed expression of SLC26A2 and FGFR3 in primary rib cartilage tissue at P0 in *Slc26a2$^{fl/lfl}$* (1), *Col2a1-Cre; Slc26a2$^{fl/fl}$* (2), *Col2a1-Cre; Slc26a2$^{fl/fl}$; Fgfr3$^{fl/fl}$* (3) mice (C) Statistical analyses of western blotting was performed with ImageJ software (D) Whole-mount skeletal staining of P0 *Slc26a2$^{fl/lfl}$* (1), *Col2a1-Cre; Slc26a2$^{fl/fl}$* (2), *Col2a1-Cre; Slc26a2$^{fl/fl}$; Fgfr3$^{fl/fl}$* (3) mice skeleton using Alizarin red and Alcian blue. Scale bar: 4 mm (E) Limbs of P0 mice. Scale bar: 2 mm (F). Statistical analysis of limb length (n = 7). For all the above-mentioned statistical analyses, significance was determined by One-way ANOVA followed by Tukey's multiple comparisons test, and the results are shown as the mean ± SD, *$P < 0.05$, **$P < 0.01$, ns: not statistically significant.

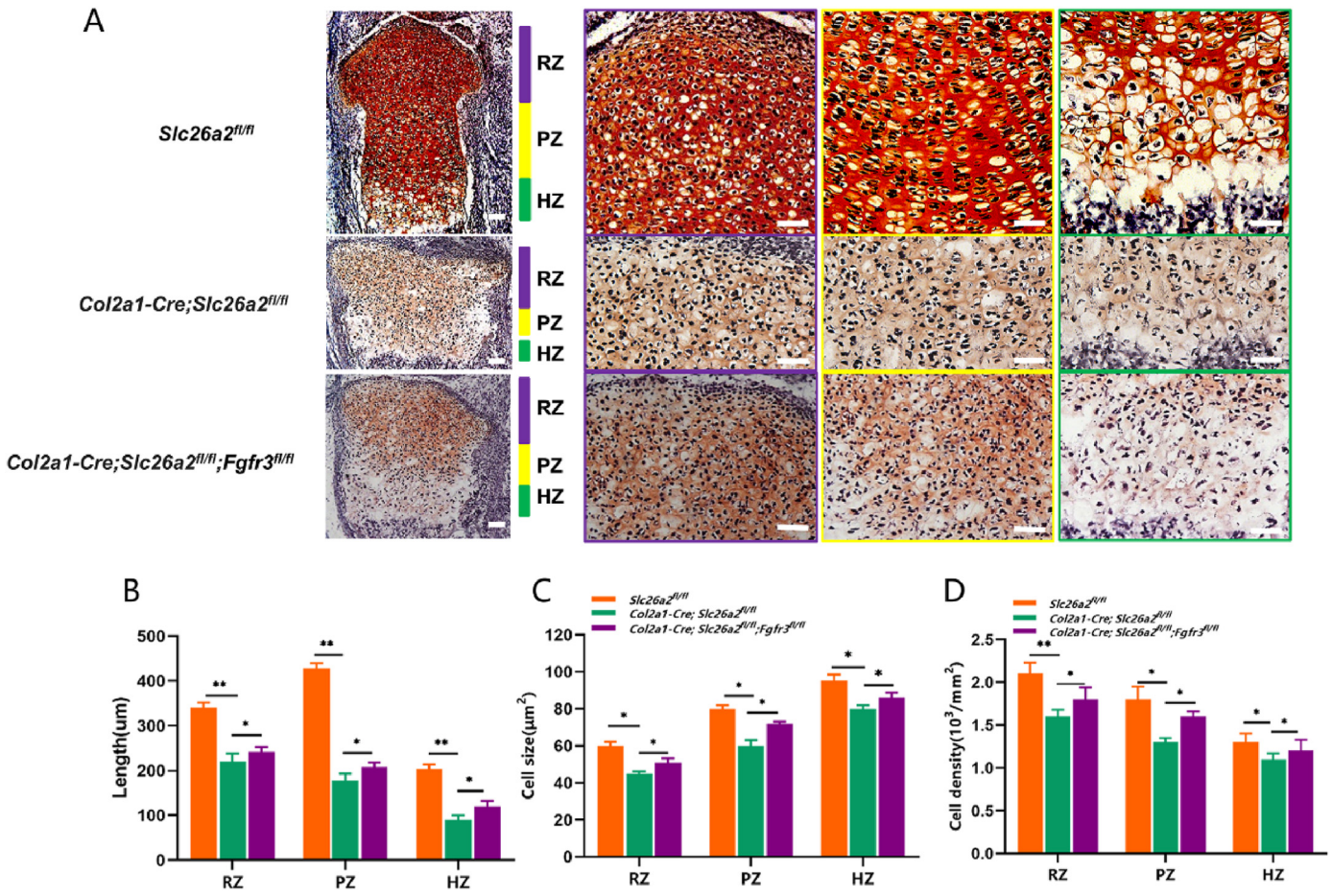

Fig. 2. Inhibition of *Fgfr3* in chondrocytes ameliorates the disorder of chondrocyte arrangement in the mouse growth plate caused by *Slc26a2* deletion (A) Safranin O and fast green staining of P0 tibial growth plates. Scale bar: 50 μm (B) (C) (D) Statistical analysis of the growth plate chondrocyte length, chondrocyte size, and chondrocyte density of the resting zone (RZ), proliferating zone (PZ), and hypertrophic zone (HZ) (n = 9/group). For all the above-mentioned statistical analyses, significance was determined by One-way ANOVA followed by Tukey's multiple comparisons test, and the results are shown as the mean ± SD, *$P < 0.05$, **$P < 0.01$.

showed a remarkable decrease in Ki67-positive cells in the proliferating region of the growth plates of *Col2a1-Cre; Slc26a2*$^{fl/fl}$ mice, indicating a reduced cell proliferation caused by *Slc26a2* deficiency. In contrast, *Col2a1-Cre; Slc26a2*$^{fl/fl}$*; Fgfr3*$^{fl/fl}$ mice exhibited significantly restored cell proliferation (Fig. 3A). Moreover, TUNEL staining showed a significantly increased number of positive cells in the hypertrophic region of the growth plates in *Col2a1-Cre; Slc26a2*$^{fl/fl}$ mice, indicating the pro-apoptotic effect of *Slc26a2* deficiency. Similarly, *Col2a1-Cre; Slc26a2*$^{fl/fl}$*; Fgfr3*$^{fl/fl}$ mice showed reduced chondrocyte apoptosis (Fig. 3B). In addition, we evaluated the phosphorylation status of ERK1/2 and STAT1, two important effectors of FGFR3 signaling that negatively regulate chondrocyte differentiation and proliferation, respectively. As expected, *Col2a1-Cre; Slc26a2*$^{fl/fl}$ mice showed a striking increase in phosphorylated ERK1/2 and STAT1 in nearly all subpopulations of growth plate chondrocytes, whereas in *Col2a1-Cre; Slc26a2*$^{fl/fl}$*; Fgfr3*$^{fl/fl}$ mice, phosphorylated ERK1/2 was more confined to chondrocytes in the hypertrophic zone, and phosphorylated STAT1 in chondrocytes was restricted to the proliferative and pre-hypertrophic zones (Fig. 3C and D). Furthermore, aberrant expression of Col X, a hallmark of specific chondrocyte hypertrophy [25], was observed in P0 growth plates of *Col2a1-Cre; Slc26a2*$^{fl/fl}$ mice compared to that in *Slc26a2*$^{fl/fl}$ mice, whereas an recovered Col X-expressing range was observed in P0 growth plates in *Col2a1-Cre; Slc26a2*$^{fl/fl}$*; Fgfr3*$^{fl/fl}$ mice (Fig. 3E). We found that Sox9, an early chondrocyte-specific marker [26], was consistently expressed during this process (Supplementary Figs. 2A and B). Our findings further confirmed that inhibition of the *Fgfr3* gene during the embryonic stage could alleviate the impairment of apoptosis and proliferation of chondrocytes in the growth plate of P0 stage mice while improving the defective differentiation of chondrocytes in the hypertrophic region.

3.3. Ablation of the Fgf3 gene in postnatal Slc26a2 mutant mice elicits a skeletal phenotype amelioration

This study used Col2a1-CreERT2; Slc26a2$^{fl/fl}$ mice to generate mice with postnatal *Slc26a2*-deficient non-lethal chondrodysplasia. A mouse model of dysplasia caused by *Slc26a2*-deficiency was generated after 5 days of continuous intraperitoneal injection of tamoxifen (TM) from 10 days after birth, and samples were collected and analyzed on P20, with Cre negativity as a control group (CTR). Subsequently, we constructed *Slc26a2* and *Fgfr3* double knockout mice based on this model, and the gross view of the mice suggested an improvement in the skeletal phenotype and a slight increase in body length (Fig. 4A–C). μCT analysis of bone development in the distal femur of mice suggested that bone mineral density (BMD), bone volume fraction (BV/TV), trabecular thickness (Tb.Th), and trabecular number (Tb.N) were reduced in the *Slc26a2* cKO mice compared with the control group, and the corresponding indicators were improved in the *Slc26a2; Fgf3* cKO group compared with the *Slc26a2* cKO mice. Similarly, there was a significant recovery in trabecular bone separation (Tb. Sp) (Fig. 4D and E). Histological staining suggested a shortened length in the resting and proliferating regions of the growth plate in *Slc26a2* cKO mice, with a loss of structural arrangement of cells in the proliferating regions and a smaller chondrocyte size in the pre-hypertrophic region. In *Slc26a2* and *Fgfr3*

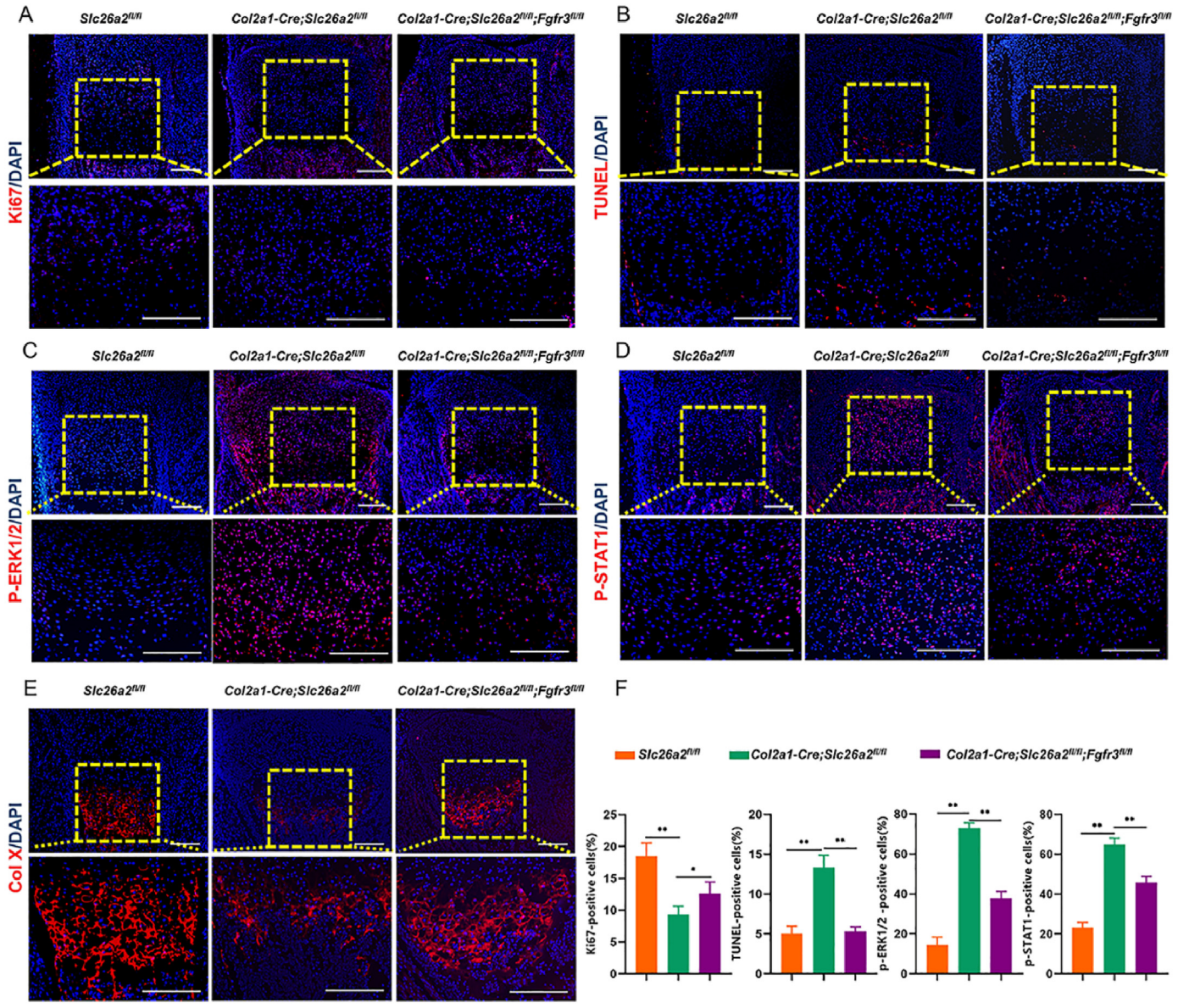

Fig. 3. Inhibition of *Fgfr3* in chondrocytes ameliorates chondrocyte proliferation apoptosis and differentiation impairment in mouse growth plate chondrocytes due to *Slc26a2* deficiency (A) (B) Ki67 immunostaining and TUNEL staining (red) of tibial sections of P0 mice. Scale bar: 50 μm (C) (D) Immunofluorescent analyses of FGFR3 signaling downstream mediators p-ERK1/2 and p-STAT1 (red) in proliferating chondrocytes of tibia sections of P0 mice. Scale bar: 50 μm (E) Immunostaining of Col X (red) of tibial sections of P0 mice (F) Quantification of Ki67-labeled cells, TUNEL-labeled cells, and p-ERK1/2- and p-STAT1-positive cells in the growth plate (n = 9/group). For all the above-mentioned statistical analyses, significance was determined by One-way ANOVA followed by Tukey's multiple comparisons test, and the results are shown as the mean ± SD, $^{*}P < 0.05$, $^{**}P < 0.01$. (For interpretation of the references to colour in this figure legend, the reader is referred to the Web version of this article.)

double-knockout mice, chondrocytes in the resting and proliferating regions were neatly arranged, and their density increased, with a well-distributed transition from the pre-hypertrophic to the hypertrophic region (Fig. 4F、G). These data suggested that ablation of *Fgf3* would also benefit postnatal *Slc26a2*-deficient non-lethal chondrodysplasia.

3.4. NVP-BGJ398 treatment enhances anabolism and proliferation in Slc26a2-deficient chondrocytes and reduces the phosphorylation downstream of FGFR3 signaling

Previously, we found that the FGFR3 inhibitor NVP-BGJ398 alleviated the dysplastic disease phenotype at the embryonic stage. However, it is unclear whether this drug directly affects *Slc26a2*-deficient chondrocytes. Therefore, we investigated whether NVP-BGJ398 mitigates defective anabolism and proliferation in *Slc26a2*-deficient chondrocytes. Primary rib chondrocytes were isolated from E18.5, *Slc26a2*$^{fl/fl}$ and *Col2a1-CreER*^{T2}, *Slc26a2*$^{fl/fl}$ mouse embryos and divided into CTR, *Slc26a2* cKO, *Slc26a2* cKO + NVP-BGJ398 groups. First, we analyzed the cytotoxic effect of NVP-BGJ398 on primary chondrocytes. Primary chondrocytes were treated with different concentrations of NVP-BGJ398 (0.1–10 μM) for 72 h; CCK8 assay showed that 10 μM NVP-BGJ398 significantly reduced cell viability. As shown in Fig. 5B, cell survival was determined using an MTT assay. Cell survival was not affected by 0.1, 1, or 5 μM NVP-BGJ treatment, but 10 μM NVP-BGJ induced cell death, and the cytotoxic effect was dose-dependent. Therefore, we selected a relatively appropriate concentration of 5 μM (Fig. 5A and B). *Slc26a2*-deficient chondrocytes showed slow growth and reduced cell volumes. After pharmacological intervention with 5 μM NVP-BGJ398, chondrocytes expanded in size and cell density increased (Fig. 5C). Alcian blue staining suggested defective acidic mucopolysaccharide

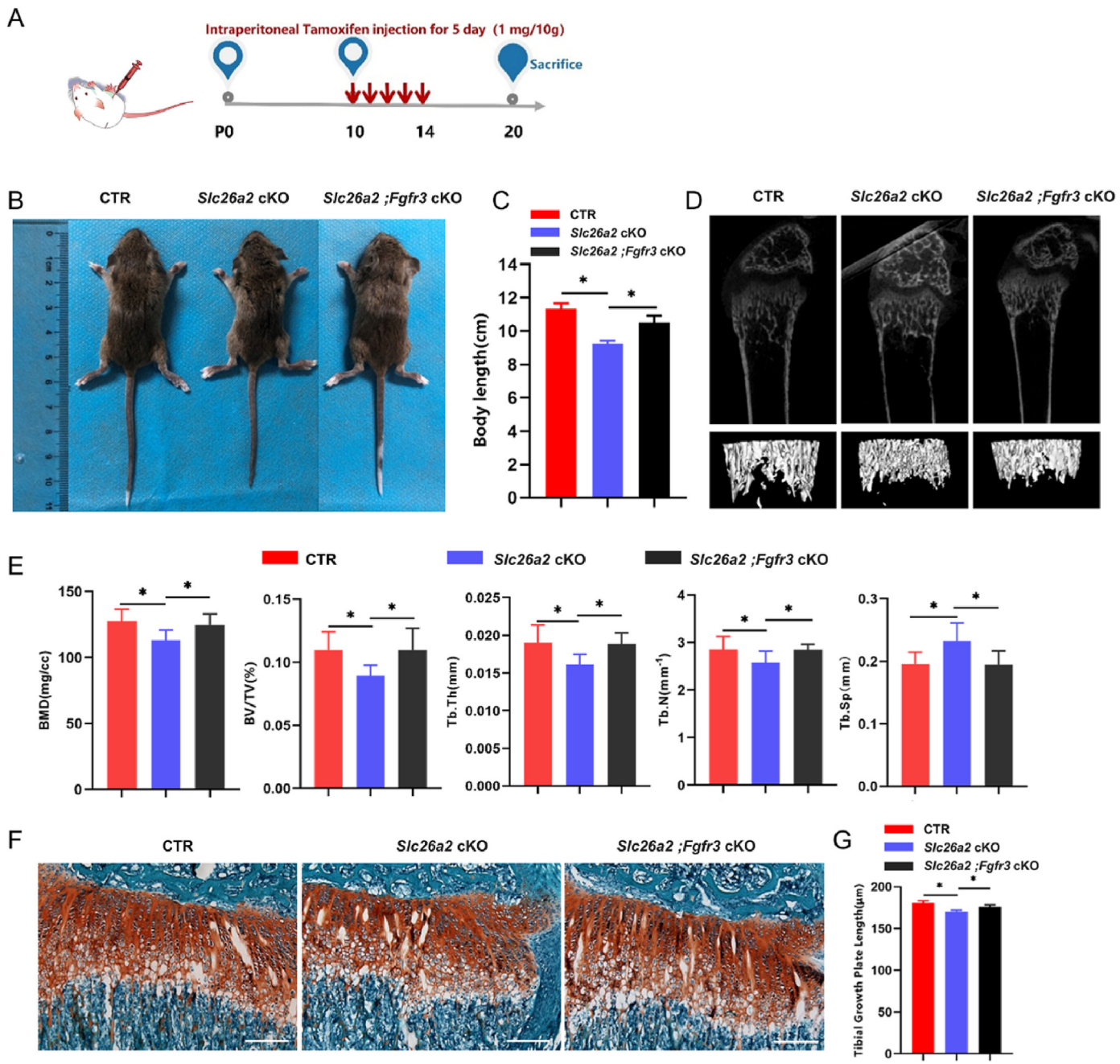

Fig. 4. *Fgf3* gene intervention slightly alleviates dysplasia caused by *Slc26a2* deficiency in P20 chondrocytes (A) Scheme of the tamoxifen (1 mg/10 g/mouse/day) injection for 5 consecutive days from day 10 and analysis on P20 (CTR, n = 7; *Slc26a2* cKO, n = 7; *Slc26a2; Fgfr3* cKO, n = 8) (B、C) Gross morphology as well as body length statistics of 20-day-old mice after tamoxifen injection (D) Micro-CT imaging of the metaphysis of the distal femur in 3D (E) Micro-CT analysis of BMD, BV/TV, Tb.Th, Tb.N, and Tb. sp of mice (F) Safranin O and fast green staining of sections of tibial growth plates at P20 and tibial growth plate length statistics. Scale bar: 100 μm. (G) Statistical analysis of growth plate length (n = 7) For all the above-mentioned statistical analyses, significance was determined by One-way ANOVA followed by Tukey's multiple comparisons test, and the results are shown as the mean ± SD, **P* < 0.05, **P < 0.01, ns: not statistically significant.

deposition in *Slc26a2*-deficient chondrocytes. Alcian blue staining increased after pharmacological intervention, suggesting an improved intracellular matrix secretion (Fig. 5D). Ki67 immunofluorescence and TUNEL staining results were consistent (Fig. 5E and F). Meanwhile, immunofluorescence and qPCR suggested that the expression of *Slc26a2*-deficient chondrogenic markers Sox9, ColII, and aggrecan decreased. This opposite response was paralleled by an increase after drug intervention (Fig. 5G–I, Supplementary Fig. 3). Treatment of cells with 5uM NVP-BGJ398 showed by immunofluorescence (Fig. 6A and B) and Western Blot analysis showed that over-activation of phosphorylation downstream of FGFR3 (p-STAT1 and p-ERK1/2) was significantly inhibited (Fig. 6C and D), correcting the chondrocyte pathological features resulting from *Slc26a2* deletion.

3.5. FGFR3 inhibitor NVP-BGJ398 ameliorates postnatal *Slc26a2*-deficient non-lethal chondrodysplasias

Col2a1-CreER^{T2}, *Slc26a2*$^{fl/fl}$ mice were used to mimic postnatal *Slc26a2*-deficient non-lethal chondrodysplasia mice, followed by subcutaneous administration of NVP-BGJ398 for a continuous period of 14 days after birth until P20 sampling. There was a significant down-regulation of p-ERK1/2 and p-STAT1 in the growth plate cartilage of

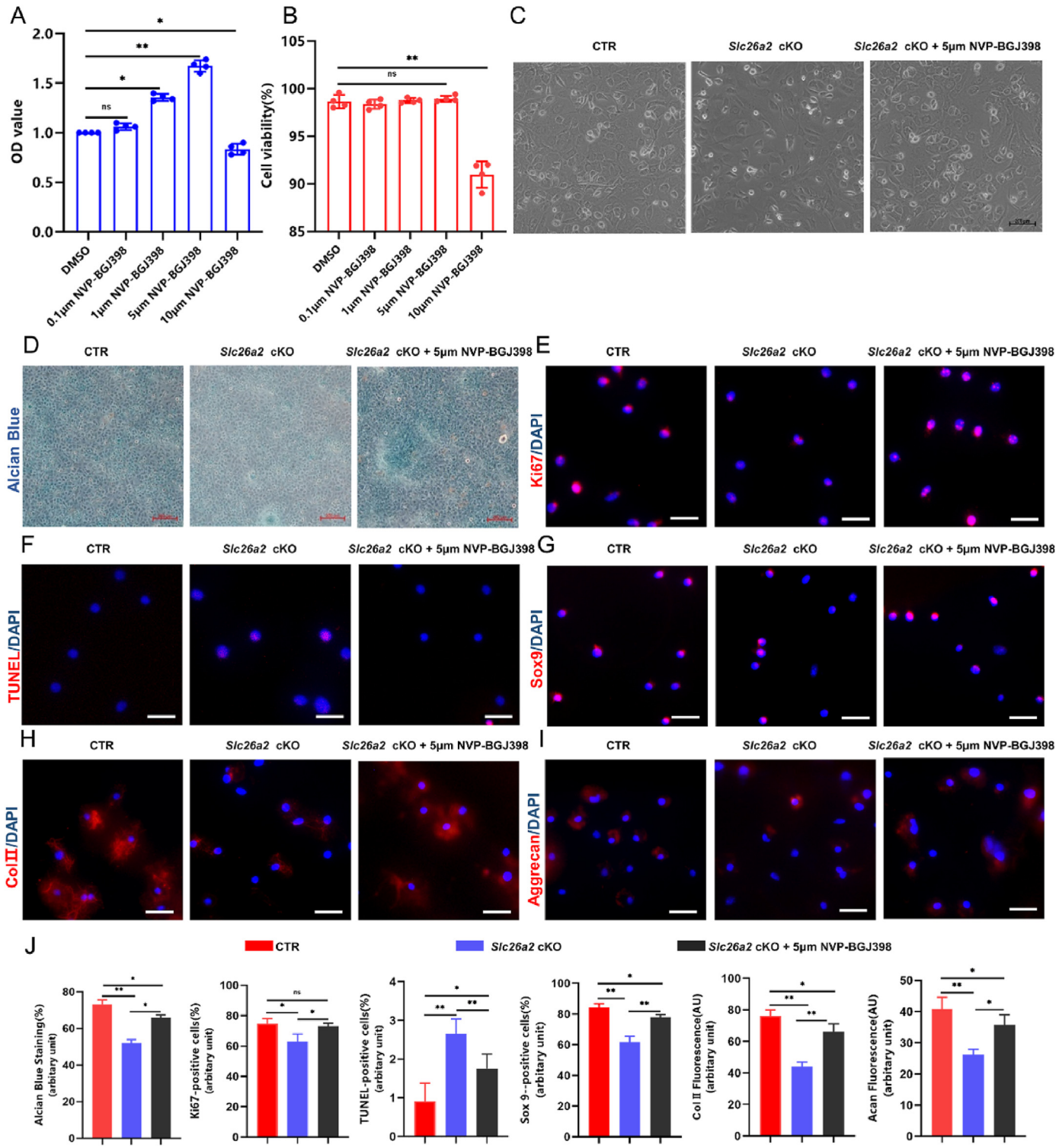

Fig. 5. *In vitro* chondrogenesis is directly modulated by NVP-BGJ398 treatment. Mouse ribbed chondrocytes were cultured and divided into 3 groups of CTR, *Slc26a2* cKO an *Slc26a2* cKO + NVP-BGJ398 (A, B) Primary chondrocytes cells were treated with different concentrations of NVP-BGJ398 (0.1–10 μM) for 72 h, CCK8 assay showed that 0.1, 1 and 5 μM NVP-BGJ treatment did not affect cell viability, but 10 μM NVP-BGJ398 significantly decreased cell viability. MTT measured cell survival, and the results showed that 0.1, 1 and 5 μM NVP-BGJ treatment did not affect cell survival, but 10 μM induced cell death with a dose-dependent cytotoxic effect (C). The representative cell morphology of each group was recorded. Scale bars, 200 μm (D) Representative images of Alcian blue-stained chondrocyte cultures. Scale bars, 100 μm (E, F) Ki67 immunostaining and TUNEL staining of chondrocytes. Scale bars, 200 μm (G–I) Immunofluorescent analyses of chondrogenic markers Sox9, ColII, and aggrecan. Scale bars, 200 μm (J) Quantification of Alcian blue staining; Ki67-, TUNEL- and Sox9-positive cells; and Col II- and aggrecan-labeled chondrocytes. For all the above-mentioned statistical analyses, significance was determined by One-way ANOVA followed by Tukey's multiple comparisons test, and the results are shown as the mean ± SD, *P < 0.05, **P < 0.01, ns: not statistically significant.

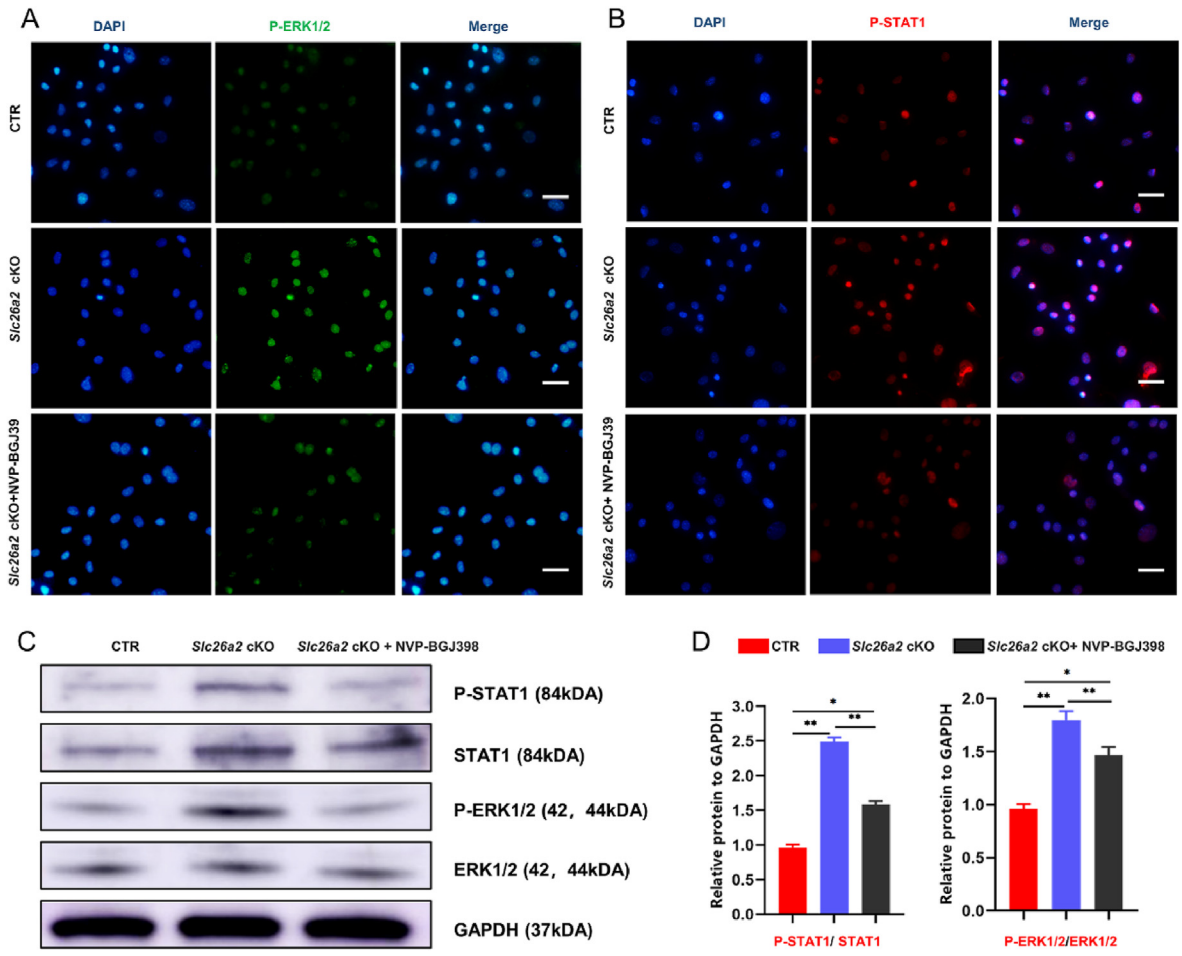

Fig. 6. NVP-BGJ398 treatment reduces the phosphorylation downstream of FGFR3 signaling in *Slc26a2*-deficient chondrocytes (A、B) p-STAT1 and p-ERK1/2 immunofluorescence staining on chondrocyte of 5 μM NVP-BGJ398-treated and –untreated cultures (C) Western blot analysis. p-STAT1 and p-ERK1/2 protein expression on chondrocytes from NVP-BGJ398 treated and untreated cultures (D) Quantitative Western blotting data from three independent experiments. For all the above-mentioned statistical analyses, significance was determined by One-way ANOVA followed by Tukey's multiple comparisons test, and the results are shown as the mean ± SD, *$P < 0.05$, **$P < 0.01$, ns: not statistically significant.

mice in the drug intervention group. However, the number of TUNEL-labeled apoptotic cells was not significantly different (Supplementary Figs. 4A–E), which could be due to the short intervention time. The phenotype had not yet recovered. Therefore, we extended the dosing cycle for observation. After sequentially administered tamoxifen and drug treatment (Fig. 7A), CTR, *Slc26a2* cKO, and *Slc26a2* cKO + NVP-BGJ398 mice were analyzed at P49 for further study. We found a significantly decreased body length of *Slc26a2* cKO mice compared with that of CTR mice, while the body length and body weight of NVP-BGJ398 treatment mice showed a significant increase (Fig. 7B, C, D). Radiological analysis showed that the lower limbs of mice with postnatal dysplasia displayed a tibial curvature phenotype consistent with the clinically reported DTD and rMED signs in humans [3,27]. Treatment with NVP-BGJ398 improved skeletal deformities at P49 (Fig. 7E and F), including tibial length and tibial bowing (genu varum: the angle between the proximal and distal heads of the tibia) [28]. We investigated whether endochondral bone formation benefits from NVP-BGJ398 treatment. Three-dimensional reconstruction images and micro-CT revealed abnormal bone parameters of bone volume in *Slc26a2* cKO mice, including BMD, BV/TV, Tb.Th, Tb.N, and Tb. Sp in the distal femur; following intervention with the drug NVP-BGJ398, mice showed significant improvement in bone indices compared to the dysplasia mice (Fig. 7G and H). These results indicated that NVP-BGJ398 may be an effective agent for the treatment of *Slc26a2*-deficient non-lethal chondrodysplasia and endochondral bone formation.

3.6. NVP-BGJ398 treatment improves chondrocyte proliferation, apoptosis, and differentiation in the growth plates of Slc26a2 cKO mice

We performed histological and fluorescence staining of tibial growth plate sections to examine chondrocyte proliferation, apoptosis, and differentiation. Safranin O staining images showed that compared with CTR mice, a reduced number and disordered arrangement of chondrocytes in the proliferative and hypertrophic zones of growth plates were observed in *Slc26a2* cKO mice, whereas NVP-BGJ398 intervention significantly restored the cell number and arrangement of chondrocytes in the growth plates (Fig. 8A). In addition, Ki67 immunofluorescence and TUNEL staining revealed a remarkable decrease in the number of Ki67-positive cells in the proliferating region and an increase in TUNEL-positive cells in the pre-hypertrophic region of the growth plates in *Slc26a2* cKO mice. As expected, NVP-BGJ398 inhibited the increase in apoptosis and promoted proliferation induced by *Slc26a2* deficiency (Fig. 8B and C). To verify whether FGFR3 signaling was involved in the therapeutic effect of NVP-BGJ398 in *Slc26a2* cKO mice, phosphorylated ERK1/2 and STAT1 were detected using immunofluorescence staining. Increased phosphorylated ERK1/2 and STAT1 were observed in the growth plates of *Slc26a2* cKO mice, whereas NVP-BGJ398 treatment significantly reduced phosphorylation of ERK1/2 and STAT1 (Fig. 8D and E). Moreover, the Col X-expressing range in the growth plate of *Slc26a2* cKO mice was significantly shorter than that in CTR mice, suggesting impaired cell differentiation induced by *Slc26a2* deficiency. In contrast, an evidently recovered

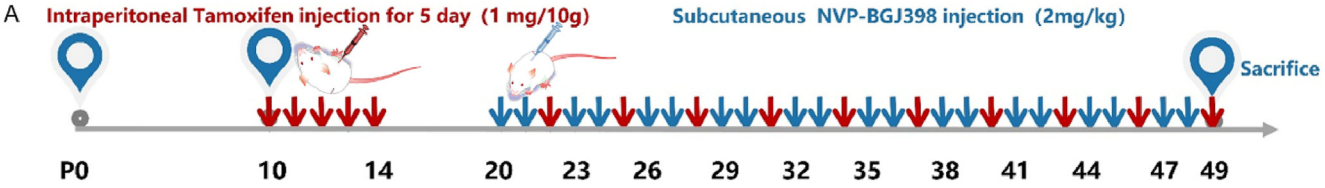

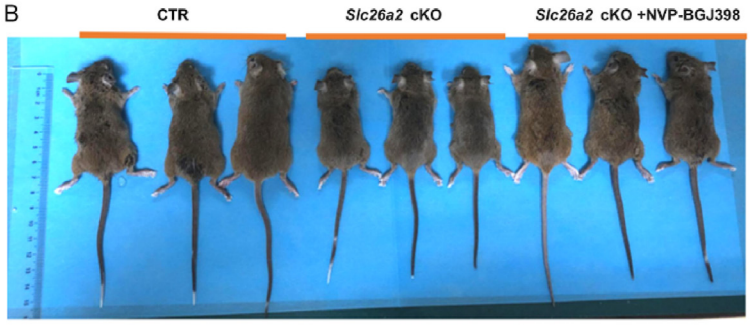

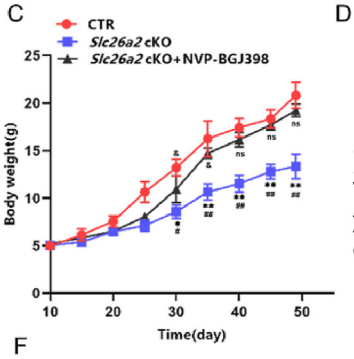

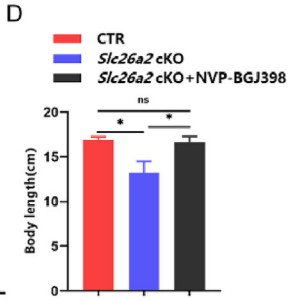

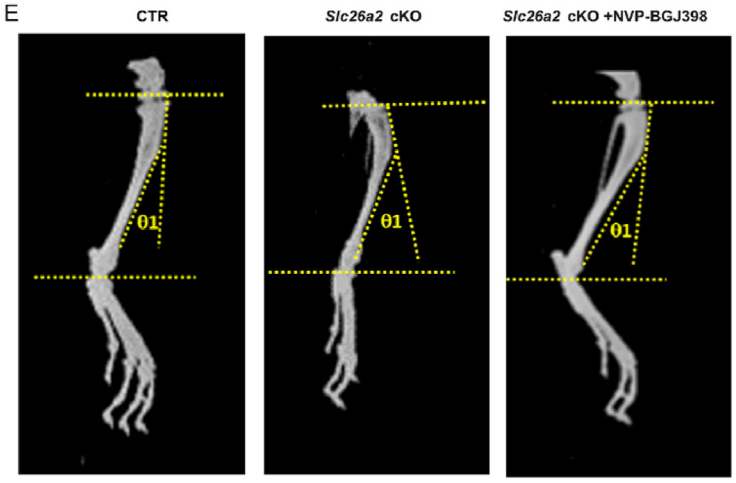

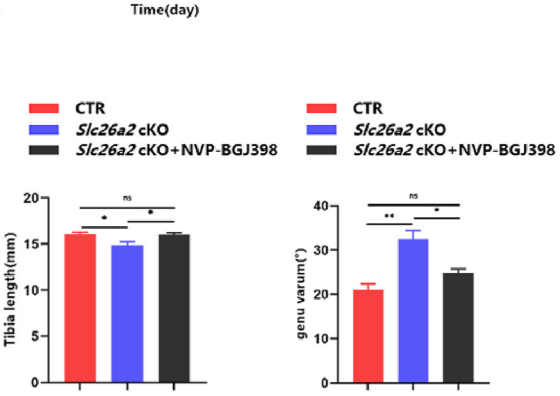

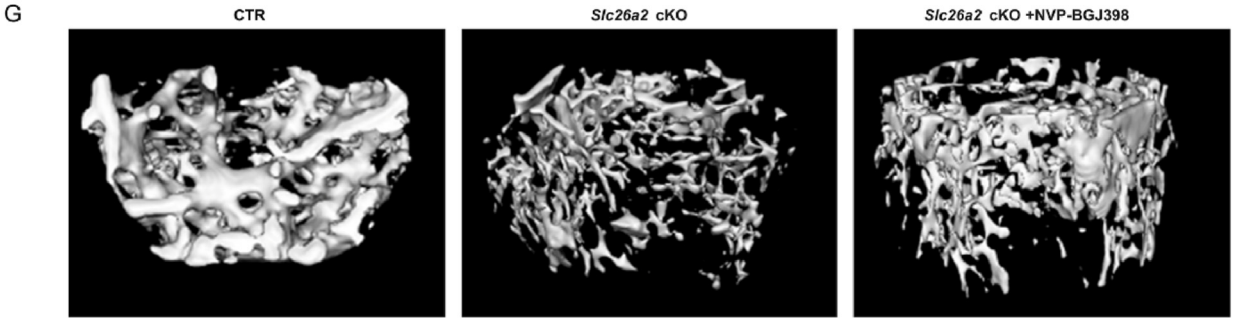

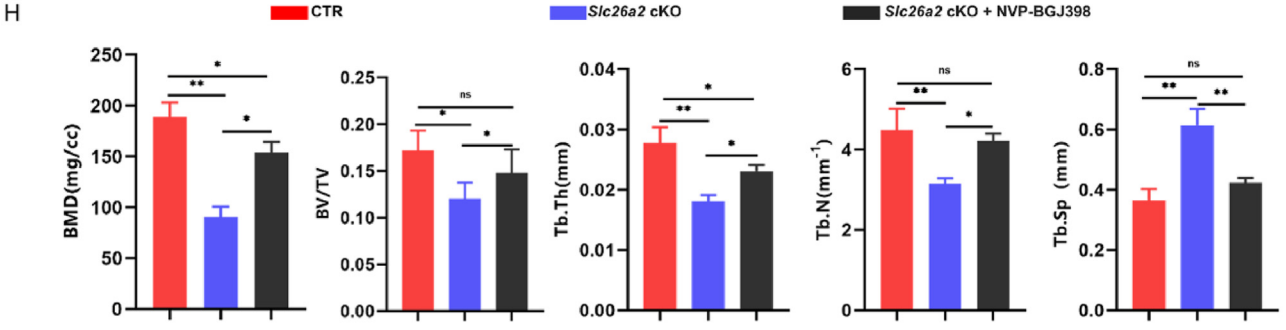

(caption on next page)

Fig. 7. FGFR3 inhibitor NVP-BGJ398 reduces the chondrodysplasia phenotype caused by *Slc26a2* deletion in chondrocytes *in vivo* (A) Scheme of the NVP-BGJ398 administration and analysis on P49. Tamoxifen (1 mg/10 g/mouse/day for 5 consecutive days from day 10). NVP-BGJ398 (2 mg/kg body weight intermittent injections every 3 days from day 20) (CTR, n = 7; *Slc26a2* cKO, n = 9, *Slc26a2* cKO + NVP-BGJ398, n = 10) (B) Gross morphology of 7-week-old mice after tamoxifen injection and NVP-BGJ398 intervention (C) Body weight was measured every 5 days and plotted (*:Slc26a2 cKO VS. CTR; #: *Slc26a2* cKO VS. *Slc26a2* cKO + NVP-BGJ398; &:CTR VS. *Slc26a2* cKO + NVP-BGJ398) (D) Body length was measured on P49 (E) Radiographic analyses revealed that skeletal deformities of chondrodysplasia were alleviated at P49 by NVP-BGJ398 treatment, including the length of tibia and genu varum (the angle between the proximal head and distal head of tibia) (F) Statistical analysis of tibia lengths and genu varum at P49 (G) Micro-CT imaging of the distal femur metaphysis in 3D (H) Micro-CT analysis of BMD, BV/TV, Tb.Th, Tb.N, and Tb. sp of mice. For all the above-mentioned statistical analyses, significance was determined by One-way ANOVA followed by Tukey's multiple comparisons test, and the results are shown as the mean ± SD, *P < 0.05, **P < 0.01, ns: not statistically significant.

Col X-expressing range was observed after intervention with NVP-BGJ398, indicating a protective effect on cell differentiation (Fig. 8F). These results further confirmed that NVP-BGJ398, a pharmacological inhibitor of FGFR3, ameliorates *Slc26a2*-deficient non-lethal chondrodysplasia by inhibiting the over-activation of the FGFR3 signaling pathway.

4. Discussion

Research on chondrodysplasia caused by SLC26A2 is limited. In our previous study, *Col2a1-Cre; Slc26a2*$^{fl/fl}$ mice mimicking lethal human chondrodysplasia disease models showed that collagen secretion was blocked in *Slc26a2*-knockout chondrocytes and significantly triggered an ATF6 pathway-mediated UPR, suggesting that this may activate the ATF6-dependent FGFR3 signaling pathway [6]. Here, we constructed double-knockout mice to confirm the *in vivo* genetic interaction between *Slc26a2* and *Fgfr3* genes in chondrocytes and observed partial alleviation of the chondrodysplasia phenotype. By constructing double knockout mice, parallel with a significant downregulation of p-ERK1/2 and p-STAT1 in the FGFR3 signaling pathway [29].

Genetic skeletal disorders (skeletal dysplasia), a rare condition with a long-term debilitating character from birth, are usually considered life-threatening, and there is no valid therapeutic option. In clinical duties, we must focus on assisting children with skeletal dysplasia and choose an appropriate time point for intervention. Therefore, we constructed a mouse disease model with tamoxifen-induced recombinant *CreER*^{T2} transgenic mice to specifically knock out *Slc26a2* in chondrocytes, which mimics the human postnatal non-lethal chondrodysplasia disease phenotype and observed excessive activation of the FGFR3 signaling pathway in this disease model.

Davide Komla-Ebri revealed that NVP-BGJ398, a PAN-FGFR inhibitor, reduced FGFR3 phosphorylation, decreased activation of downstream signaling pathways in human and mouse *FGFR3*$^{Y367C/+}$ chondrocytes *in vitro*, and rescued the abnormal phenotype of growth plate development *in vivo* [14]. Here, we simultaneously knocked down *Fgfr3*, which was found to alleviate dysplasia at the P20 stage. We then performed a short-term pharmacological NVP-BGJ398 intervention and found a weak improvement in the phenotype of the mice. To investigate whether more prolonged treatment with NVP-BGJ398 could improve the dysplastic phenotype, we extended the duration of the intervention and observed a significant increase in body size in *Slc26a2* cKO mice at 49 days postnatally. Short-limb dwarfism and genu valgum are the most common childhood skeletal dysplasia disorders, and the mouse model we constructed replicated this phenotype in humans [30]. Roberta Besio et al. noted that impaired proliferation and accelerated apoptosis in the chondrocyte proliferative region were significantly associated with maturation in the hypertrophic region, reducing bone growth, and found that deficiency of an enzyme that participates in collagen synthesis and degradation (prolidase) severely affects bone formation, leading to a skeletal phenotype of short stature with genu valgum [31]. Shaukat Khan et al. showed that abnormal accumulation of glycosaminoglycans in the cartilage and extracellular matrix directly affects cartilage and bone development, typically characterized by hip valgus and genu valgum [32]. Surprisingly, our study revealed that pharmacological intervention improved the phenotype of tibial skeletal length and curvature deformities in mice, which is consistent with the results of several published experiments on FGFR3 causing dwarfism [6,33,34]. The micro-CT of mouse femurs showed improvements in BMD, BV/TV, Tb.Th, and Tb.N, a reduction in Tb. Sp after NVP-BGJ398 intervention and the developmental growth status of some mice exceeded that of normal controls after drug intervention, which may be related to improved endochondral ossification after the restoration of FGFR3 signaling [35].

The tyrosine kinase inhibitor NVP-BGJ398 directly inhibits the phosphorylation of FGFR3 [36–39]. Several recent clinical trials have evaluated the long-term effects of NVP-BGJ398 and the pharmacokinetics of its metabolic activities, confirming its safety and efficacy in treating children with dysplasia [15,38,40]. Therefore, NVP-BGJ398 represents a straightforward therapeutic strategy to counteract the overactivation of FGFR3 in pathological situations, and FGFR3-inhibiting small-molecule drugs could be repurposed for the treatment of *Slc26a2*-related chondrodysplasia disorders in the future. However, it is worth noting that the dose of NVP-BGJ398 used for oncologic indications is considerably higher than that used in the current skeletal development clinical trials. The characteristics of low doses of NVP-BGJ398 in pediatric patients with chondrodysplasia and the appropriate therapeutic dosage still need to be determined.

In addition to this study, Rossi found a reduction in sulfated proteoglycan synthesis in the systemic knock-in mutation of *dtd* mice, owing to low intracellular sulfate levels [41]. Therefore, N-acetylcysteine (NAC) was selected as an alternative to intracellular sulfate to improve the phenotype of postnatal skeletal dysplasia in *dtd* mice [42–44]. Endoplasmic reticulum (ER) stress is also becoming a unifying disease mechanism for targeting certain diseases (rMED), particularly skeletal dysplasia. Targeting ER stress through pharmacological repurposing has also emerged as an appealing approach that has been successfully applied to the treatment of metaphyseal chondrodysplasia type Schmid (MCDS) associated with collagen type X defects [45,46]. Instead, our study brings forward another therapeutic strategy by drugging pathogenic FGFR3 signaling with NVP-BGJ398, which could elicit skeletal phenotype amelioration at the morphological and histological levels.

Drug repositioning is an innovative alternative to the drug development process, expanding the drug's original scope of application and utility and significantly reducing the time and cost of new drug exploration [47,48]. Accordingly, our data provided genetic and pharmacological evidence to support that targeting FGFR3 signaling by NVP-BGJ398 could be a route for the treatment of SLC26A2-associated skeletal disorders, which could hopefully advance therapeutic development.

Author contributions

Pan Li, Zhuojing Luo and Liu Yang designed the research; **Pan Li** screened all the primary literature and analyzed the presented experimental data; **Pan Li, Dong Wang, Weiguang Lu, Xin He, Jingyan Hu, Haitao Yun and Chengxiang Zhao** discussed the data; **Pan Li and Liu Yang** wrote the paper; **Liu Yang and Qiang Jie** revised the manuscript. All authors reviewed and approved the final manuscript.

Funding

This work was supported by the National Natural Science Foundation of China (81871743, 82020108019, and 82272442), Innovation Team

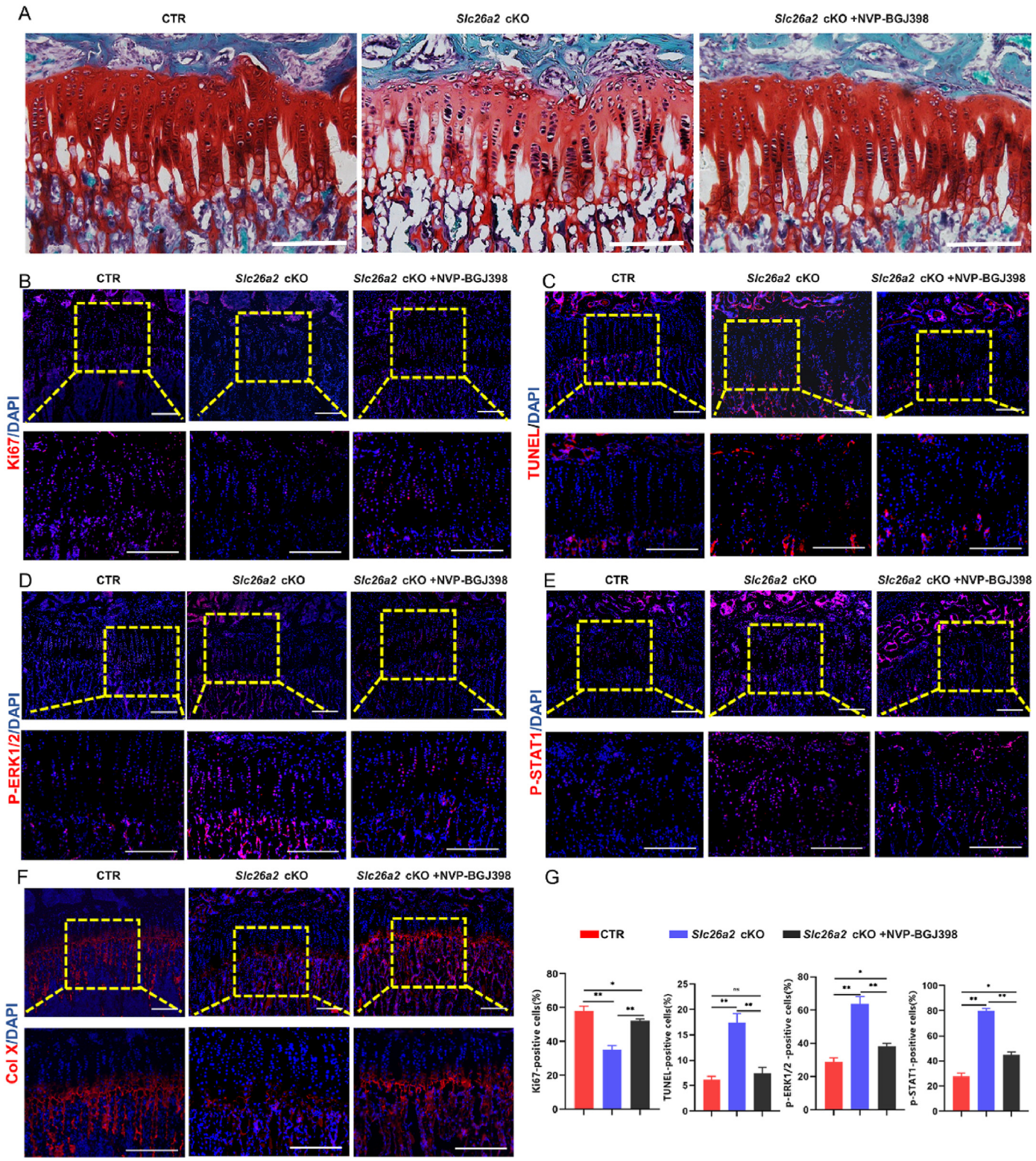

Fig. 8. NVP-BGJ398 pharmacological intervention inhibits overactivation of the FGFR3 signaling pathway in *Slc26a2* cKO mice (A) Safranin O and fast green staining of sections of tibial growth plates at P49. Slightly increased proliferating and hypertrophic chondrocytes were observed in NVP-BGJ398-treated growth plates compared with those of tamoxifen-induced chondrodysplasia groups. Scale bar: 100 μm (B) (C) Ki67 immunostaining and TUNEL staining (red) of tibia sections on P49. Scale bar: 50 μm (D) (E) Immunofluorescent analyses of FGFR3 signaling downstream mediators p-ERK1/2 and p-STAT1 (red) in growth plate chondrocytes on tibia sections at P49. Scale bar: 50 μm (F) Immunostaining of Col X (red) on tibia sections (G) Quantification of Ki67-labeled cells, TUNEL-labeled cells, and p-ERK1/2- and p-STAT1-positive cells in the growth plate (n = 7). For all the above-mentioned statistical analyses, significance was determined by One-way ANOVA followed by Tukey's multiple comparisons test, and the results are shown as the mean ± SD, *P < 0.05, **P < 0.01, ns: not statistically significant.

Projects – Innovation Capability Support Program of Shaanxi Province (2020TD-036), and the Key Industrial Chain Program of Shaanxi (2022ZDLSF02-12). The funder had no role in the study design, data collection, data analysis, interpretation, or manuscript writing. We would like to thank Editage (www.editage.cn) for the English language editing.

Ethics Statement: The animal study was reviewed and approved by the Animal Research Ethics Committee of the Fourth Military Medical University.

Declaration of competing interest

There is no conflict of interests to report, and all authors have conformed to all the editorial policies of *Journal of Orthopaedic Translation.*

Appendix A. Supplementary data

Supplementary data to this article can be found online at https://doi.org/10.1016/j.jot.2023.09.003.

References

[1] Park M, Ohana E, Choi SY, Lee MS, Park JH, Muallem S. Multiple roles of the SO4(2-)/Cl-/OH- exchanger protein Slc26a2 in chondrocyte functions. J Biol Chem 2014;289(4):1993–2001.
[2] Cai T, Yang L, Cai W, Guo S, Yu P, Li J, et al. Dysplastic spondylolysis is caused by mutations in the diastrophic dysplasia sulfate transporter gene. Proc Natl Acad Sci U S A 2015;112(26):8064–9.
[3] Härkönen H, Loid P, Mäkitie O. SLC26A2-Associated diastrophic dysplasia and rMED-clinical features in affected Finnish children and review of the literature. Genes 2021;12(5).
[4] Rossi A, Superti-Furga A. Mutations in the diastrophic dysplasia sulfate transporter (DTDST) gene (SLC26A2): 22 novel mutations, mutation review, associated skeletal phenotypes, and diagnostic relevance. Hum Mutat 2001;17(3):159–71.
[5] Mertz EL, Facchini M, Pham AT, Gualeni B, De Leonardis F, Rossi A, et al. Matrix disruptions, growth, and degradation of cartilage with impaired sulfation. J Biol Chem 2012;287(26):22030–42.
[6] Zheng C, Lin X, Xu X, Wang C, Zhou J, Gao B, et al. Suppressing UPR-dependent overactivation of FGFR3 signaling ameliorates SLC26A2-deficient chondrodysplasias. EBioMedicine 2019;40:695–709.
[7] Miyake A, Nishimura G, Futami T, Ohashi H, Chiba K, Toyama Y, et al. A compound heterozygote of novel and recurrent DTDST mutations results in a novel intermediate phenotype of Desbuquois dysplasia, diastrophic dysplasia, and recessive form of multiple epiphyseal dysplasia. J Hum Genet 2008;53(8):764–8.
[8] Karniski LP. Functional expression and cellular distribution of diastrophic dysplasia sulfate transporter (DTDST) gene mutations in HEK cells. Hum Mol Genet 2004;13(19):2165–71.
[9] Forlino A, Piazza R, Tiveron C, Della Torre S, Tatangelo L, Bonafè L, et al. A diastrophic dysplasia sulfate transporter (SLC26A2) mutant mouse: morphological and biochemical characterization of the resulting chondrodysplasia phenotype. Hum Mol Genet 2005;14(6):859–71.
[10] De Leonardis F, Monti L, Gualeni B, Tenni R, Forlino A, Rossi A. Altered signaling in the G1 phase deregulates chondrocyte growth in a mouse model with proteoglycan undersulfation. J Cell Biochem 2014;115(10):1779–86.
[11] Chew NJ, Nguyen EV, Su SP, Novy K, Chan HC, Nguyen LK, et al. FGFR3 signaling and function in triple negative breast cancer. Cell Commun Signal 2020;18(1):13.
[12] Taieb M, Ghannoum D, Barré L, Ouzzine M. Xylosyltransferase I mediates the synthesis of proteoglycans with long glycosaminoglycan chains and controls chondrocyte hypertrophy and collagen fibers organization of in the growth plate. Cell Death Dis 2023;14(6):355.
[13] Javle M, Lowery M, Shroff RT, Weiss KH, Springfeld C, Borad MJ, et al. Phase II study of BGJ398 in patients with FGFR-altered advanced cholangiocarcinoma. J Clin Oncol 2018;36(3):276–82.
[14] Komla-Ebri D, Dambroise E, Kramer I, Benoist-Lasselin C, Kaci N, Le Gall C, et al. Tyrosine kinase inhibitor NVP-BGJ398 functionally improves FGFR3-related dwarfism in mouse model. J Clin Invest 2016;126(5):1871–84.
[15] Savarirayan R, De Bergua JM, Arundel P, McDevitt H, Cormier-Daire V, Saraff V, et al. Infigratinib in children with achondroplasia: the PROPEL and PROPEL 2 studies. Ther Adv Musculoskelet Dis 2022;14. 1759720x221084848.
[16] Su N, Xu X, Li C, He Q, Zhao L, Li C, et al. Generation of Fgfr3 conditional knockout mice. Int J Biol Sci 2010;6(4):327–32.
[17] Yan B, Zhang Z, Jin D, Cai C, Jia C, Liu W, et al. mTORC1 regulates PTHrP to coordinate chondrocyte growth, proliferation and differentiation. Nat Commun 2016;7:11151.
[18] Yang H, Zhang M, Liu Q, Zhang H, Zhang J, Lu L, et al. Inhibition of ihh reverses temporomandibular joint osteoarthritis via a PTH1R signaling dependent mechanism. Int J Mol Sci 2019;20(15).
[19] Rigueur D, Lyons KM. Whole-mount skeletal staining. Methods Mol Biol 2014;1130:113–21.
[20] Alibegović A, Blagus R, Martinez IZ. Safranin O without fast green is the best staining method for testing the degradation of macromolecules in a cartilage extracellular matrix for the determination of the postmortem interval. Forensic Sci Med Pathol 2020;16(2):252–8.
[21] Crowley LC, Marfell BJ, Waterhouse NJ. Detection of DNA fragmentation in apoptotic cells by TUNEL. Cold Spring Harb Protoc 2016;2016(10).
[22] Zheng C, Lin X, Liu H, Lu W, Xu X, Wang D, et al. Phenotypic characterization of Slc26a2 mutant mice reveals a multifactorial etiology of spondylolysis. Faseb J 2020;34(1):720–34.
[23] Chen M, Lichtler AC, Sheu TJ, Xie C, Zhang X, O'Keefe RJ, et al. Generation of a transgenic mouse model with chondrocyte-specific and tamoxifen-inducible expression of Cre recombinase. Genesis 2007;45(1):44–50.
[24] Ustun S, Tombuloglu A, Kilinc M, Guler MO, Tekinay AB. Growth and differentiation of prechondrogenic cells on bioactive self-assembled peptide nanofibers. Biomacromolecules 2013;14(1):17–26.
[25] Choi H, Tessier S, Silagi ES, Kyada R, Yousefi F, Pleshko N, et al. A novel mouse model of intervertebral disc degeneration shows altered cell fate and matrix homeostasis. Matrix Biol 2018;70:102–22.
[26] Nalesso G, Thorup AS, Eldridge SE, De Palma A, Kaur A, Peddireddi K, et al. Calcium calmodulin kinase II activity is required for cartilage homeostasis in osteoarthritis. Sci Rep 2021;11(1):5682.
[27] Mäkitie O, Geiberger S, Horemuzova E, Hagenäs L, Moström E, Nordenskjöld M, et al. SLC26A2 disease spectrum in Sweden - high frequency of recessive multiple epiphyseal dysplasia (rMED). Clin Genet 2015;87(3):273–8.
[28] Wang C, Tan Z, Niu B, Tsang KY, Tai A, Chan WCW, et al. Inhibiting the integrated stress response pathway prevents aberrant chondrocyte differentiation thereby alleviating chondrodysplasia. Elife 2018;7.
[29] Montone R, Romanelli MG, Baruzzi A, Ferrarini F, Liboi E, Lievens PM. Mutant FGFR3 associated with SADDAN disease causes cytoskeleton disorganization through PLCγ1/Src-mediated paxillin hyperphosphorylation. Int J Biochem Cell Biol 2018;95:17–26.
[30] Zechi-Ceide RM, Moura PP, Raskin S, Richieri-Costa A, Guion-Almeida ML. A compound heterozygote SLC26A2 mutation resulting in robin sequence, mild limbs shortness, accelerated carpal ossification, and multiple epiphysial dysplasia in two Brazilian sisters. A new intermediate phenotype between diastrophic dysplasia and recessive multiple epiphyseal dysplasia. Am J Med Genet 2013;161a(8):2088–94.
[31] Besio R, Maruelli S, Gioia R, Villa I, Grabowski P, Gallagher O, et al. Lack of prolidase causes a bone phenotype both in human and in mouse. Bone 2015;72:53–64.
[32] Khan S, Alméciga-Díaz CJ, Sawamoto K, Mackenzie WG, Theroux MC, Pizarro C, et al. Mucopolysaccharidosis IVA and glycosaminoglycans. Mol Genet Metabol 2017;120(1–2):78–95.
[33] Biosse Duplan M, Komla-Ebri D, Heuzé Y, Estibals V, Gaudas E, Kaci N, et al. Meckel's and condylar cartilages anomalies in achondroplasia result in defective development and growth of the mandible. Hum Mol Genet 2016;25(14):2997–3010.
[34] Gudernova I, Vesela I, Balek L, Buchtova M, Dosedelova H, Kunova M, et al. Multikinase activity of fibroblast growth factor receptor (FGFR) inhibitors SU5402, PD173074, AZD1480, AZD4547 and BGJ398 compromises the use of small chemicals targeting FGFR catalytic activity for therapy of short-stature syndromes. Hum Mol Genet 2016;25(1):9–23.
[35] Qin X, Jiang Q, Komori H, Sakane C, Fukuyama R, Matsuo Y, et al. Runt-related transcription factor-2 (Runx2) is required for bone matrix protein gene expression in committed osteoblasts in mice. J Bone Miner Res 2021;36(10):2081–95.
[36] Lima NC, Atkinson E, Bunney TD, Katan M, Huang PH. Targeting the src pathway enhances the efficacy of selective FGFR inhibitors in urothelial cancers with FGFR3 alterations. Int J Mol Sci 2020;21(9).
[37] Pal SK, Rosenberg JE, Hoffman-Censits JH, Berger R, Quinn DI, Galsky MD, et al. Efficacy of BGJ398, a fibroblast growth factor receptor 1-3 inhibitor, in patients with previously treated advanced urothelial carcinoma with FGFR3 alterations. Cancer Discov 2018;8(7):812–21.
[38] Pal SK, Somford DM, Grivas P, Sridhar SS, Gupta S, Bellmunt J, et al. Targeting FGFR3 alterations with adjuvant infigratinib in invasive urothelial carcinoma: the phase III PROOF 302 trial. Future Oncol 2022;18(21):2599–614.
[39] Botrus G, Raman P, Oliver T, Bekaii-Saab T. Infigratinib (BGJ398): an investigational agent for the treatment of FGFR-altered intrahepatic cholangiocarcinoma. Expet Opin Invest Drugs 2021;30(4):309–16.
[40] Lassman AB, Sepúlveda-Sánchez JM, Cloughesy TF, Gil-Gil MJ, Puduvalli VK, Raizer JJ, et al. Infigratinib in patients with recurrent gliomas and FGFR alterations: a multicenter phase II study. Clin Cancer Res 2022;28(11):2270–7.
[41] Paganini C, Costantini R, Rossi A. Analysis of proteoglycan synthesis and secretion in cell culture systems. Methods Mol Biol 2019;1952:71–80.
[42] Monti L, Paganini C, Lecci S, De Leonardis F, Hay E, Cohen-Solal M, et al. N-acetylcysteine treatment ameliorates the skeletal phenotype of a mouse model of diastrophic dysplasia. Hum Mol Genet 2015;24(19):5570–80.
[43] Paganini C, Gramegna Tota C, Monti L, Monti I, Maurizi A, Capulli M, et al. Improvement of the skeletal phenotype in a mouse model of diastrophic dysplasia after postnatal treatment with N-acetylcysteine. Biochem Pharmacol 2021;185:114452.
[44] Pecora F, Gualeni B, Forlino A, Superti-Furga A, Tenni R, Cetta G, et al. In vivo contribution of amino acid sulfur to cartilage proteoglycan sulfation. Biochem J 2006;398(3):509–14.
[45] Dennis EP, Greenhalgh-Maychell PL, Briggs MD. Multiple epiphyseal dysplasia and related disorders: molecular genetics, disease mechanisms, and therapeutic avenues. Dev Dynam 2021;250(3):345–59.

[46] Mullan LA, Mularczyk EJ, Kung LH, Forouhan M, Wragg JM, Goodacre R, et al. Increased intracellular proteolysis reduces disease severity in an ER stress-associated dwarfism. J Clin Invest 2017;127(10):3861–5.
[47] Chen J, Li Y, Wang S, Zhang H, Du Y, Wu Q, et al. Targeting Clostridioides difficile: new uses for old drugs. Drug Discov Today 2022;27(7):1862–73.
[48] Wang KD, Ding X, Jiang N, Zeng C, Wu J, Cai XY, et al. Digoxin targets low density lipoprotein receptor-related protein 4 and protects against osteoarthritis. Ann Rheum Dis 2022;81(4):544–55.